

PAPER

Introduction of a 3×4 Mueller matrix decomposition method

To cite this article: Mariacarla Gonzalez *et al* 2021 *J. Phys. D: Appl. Phys.* **54** 424005

View the [article online](#) for updates and enhancements.


The image shows a promotional banner for IOP ebooks. On the left, there is a collage of colorful book covers, including one titled 'Infrared Imaging: A handbook for clinical medicine'. The right side of the banner has a grey background with the text 'IOP | ebooks™' in red and black. Below the logo, it says 'Bringing together innovative digital publishing with leading authors from the global scientific community.' and 'Start exploring the collection—download the first chapter of every title for free.'

IOP | ebooks™

Bringing together innovative digital publishing with leading authors from the global scientific community.

Start exploring the collection—download the first chapter of every title for free.

Introduction of a 3×4 Mueller matrix decomposition method

Mariacarla Gonzalez¹ , Razvigor Ossikovski³ , Tatiana Novikova³ 
and Jessica C Ramella-Roman^{1,2,*} 

¹ Biomedical Engineering Department, Florida International University, 10555 W Flagler St, Miami, FL 33174, United States of America

² Department of Ophthalmology, Florida International University, Herbert Wertheim College of Medicine Cellular Biology and Pharmacology, Miami, FL 33174, United States of America

³ LPICM, CNRS, Ecole polytechnique, IP Paris, France, 91128 Palaiseau, France

E-mail: jramella@fiu.edu

Received 8 April 2021, revised 18 May 2021

Accepted for publication 20 July 2021

Published 3 August 2021



CrossMark

Abstract

A Mueller matrix can completely characterize the polarimetric properties of a medium, where the parameters of depolarization, retardance and diattenuation can be obtained by decomposing a Mueller matrix with existing decomposition methods. The introduction of polarization sensitive cameras with integrated wire-grid polarizers has allowed for the fast acquisition and analysis of four linear states within a single snapshot. Moreover, these cameras provide the opportunity to capture a reduced 3×4 Mueller matrix with the acquisition of generated states polarization in the illumination arm. In order to measure and characterize samples using a reduced 3×4 Mueller matrix, a 3×4 decomposition algorithm is introduced. This new algorithm is compared and validated against established 4×4 decompositions. The validation of this algorithm is shown using a previously reported Mueller matrix of polyacrylamide phantom, and experimental Mueller matrices of quarter-wave plates, silicone phantoms and a skin model sample. The 3×4 decomposition compares well to established decompositions and is capable of characterizing the samples based on the calculation of depolarization, retardance and orientation.

Keywords: Mueller matrix, Mueller matrix decomposition, polarimetry

(Some figures may appear in colour only in the online journal)

1. Introduction

A 4×4 Mueller matrix describes the polarization transfer function [1, 2] of any medium using 16 parameters where the medium's polarization properties are encoded [3, 4]. Several methods have been proposed to experimentally measure a Mueller matrix [5] of different media. Recently, polarization sensitive cameras that integrate 4-directional wire-grid polarizers within the sensitive area have been introduced [6, 7]. These snapshot systems can speed the acquisition process of reduced 3×4 Mueller matrix polarimetry by acquiring four different linear states of polarization (0° , 45° , 90° , 135° with

respect to a reference plane) simultaneously. Studies aimed at understanding the accuracy and limitations of these cameras have been published [6, 8–11]. The polarization sensitive cameras have been used in applications ranging from navigation [12, 13] to biological media analysis. For example, the camera has been successfully used to observe and analyze polarimetric changes of dehydrated bovine tissues [7] and they have been integrated into rigid endoscopes [14].

Mueller Matrix decomposition is used to obtain a better understanding of a material properties. There are various established 4×4 Mueller matrix decomposition methods to extract the parameters of depolarization, retardation and diattenuation from a full Mueller matrix.

The polar decomposition or Lu-Chipman (LC) decomposition [15] defines the Mueller matrix as a product of three

* Author to whom any correspondence should be addressed.

matrices: a depolarizer (M_Δ), a retarder (M_R) and a diattenuation (M_D) matrix:

$$M = M_\Delta M_R M_D. \quad (1)$$

The order of decomposition affects the result due to the non-commuting properties of matrix multiplication [16], therefore other sequential matrix decompositions have been suggested. There has been introduced a reverse decomposition [17]:

$$M = M_D M_R M_{\Delta r}, \quad (2)$$

where $M_{\Delta r}$ describes a depolarizer with diattenuation (in contrast with the M_Δ parameter in the LC decomposition being a depolarizer with polarizance).

Ossikovski proposed the symmetric decomposition [18], that introduces the idea that the depolarizer matrix could be placed 'in the middle' of retarder and diattenuation matrices:

$$M = M_{D2} M_{R2} M_{\Delta d} M_{R1} M_{D1}, \quad (3)$$

where M_{D1} and M_{D2} are two diattenuator matrices, M_{R1} and M_{R2} are two retarder matrices and $M_{\Delta d}$ is the pure depolarizer matrix.

This decomposition is particularly relevant for a backscattering configuration where the polarimetric effects (diattenuation and retardance) will occur in the forward direction of light propagation as well as in the backward path [19].

Moreover, there is also a differential (D) decomposition [20, 21] where the three polarimetric properties are considered to be occurring simultaneously and therefore can all be represented in one single differential matrix:

$$m = (dM_z/dz) M_z^{-1}, \quad (4)$$

in response to the advent of polarization sensitive camera a reduced 3×3 Mueller matrix decomposition has been introduced [22, 23]. When the measurement configuration allows for only linear states to be generated and analyzed, only nine coefficients of the upper left 3×3 submatrix of a full Mueller matrix can be acquired. This 3×3 Mueller submatrix decomposition follows a similar procedure as the LC decomposition of a full 4×4 Mueller matrix making the assumption that the depolarization of the linearly polarized light isotropic, i.e. it does not depend on the incident linear polarization vector orientation [22]. This decomposition has been used in the polarimetric studies of samples, such as aqueous suspension of polystyrene microspheres and *ex vivo* rat abdomen, although the quantitative disparities between the 3×3 and 4×4 decompositions have been reported [24].

In this paper we introduce the use of a polarization camera as a (standalone) polarization state analyzer (PSA) along with a four-state polarization state generator (PSG), for the measurements of a reduced 3×4 Mueller matrix and a new decomposition algorithm of this reduced 3×4 matrix with the aim of improving accuracy of the latter decomposition and its validation by the 4×4 decomposition results.

2. Methods

In the symmetric decomposition of a Mueller matrix (equation (3)) M_{D1} and M_{D2} are the Mueller matrices of the entrance and exit diattenuators, M_{R1} and M_{R2} are the Mueller matrices entrance and exit retarders, respectively, and M_Δ is the diagonal matrix of a canonical depolarizer.

M_Δ is defined as:

$$M_\Delta = \begin{bmatrix} 1 & 0 & 0 & 0 \\ 0 & d_1 & 0 & 0 \\ 0 & 0 & d_2 & 0 \\ 0 & 0 & 0 & d_3 \end{bmatrix}, \quad (5)$$

with a depolarization power Δ that is defined as:

$$\Delta = 1 - \frac{|d_1| + |d_2| + |d_3|}{3}, \quad (6)$$

where d_1 and d_2 are the depolarization coefficients for the linear states (horizontal/vertical and 45/135, respectively) and d_3 is the depolarization coefficient for the circular states. The Δ parameter ranges from 0 to 1, where $\Delta = 0$ is for a nondepolarizing sample.

In close to normal reflection, the following assumptions hold: $M_{D1} \approx M_{D2} \approx I$, where I is the identity matrix.

This assumption is legitimate whenever the surface contribution to diattenuation dominates compared to the volume contribution (these are the first surface in reflection or both surfaces in transmission), since Fresnel reflection and transmission coefficients coincide for both s and p polarizations at normal incidence ($r_p \approx r_s$; $t_p \approx t_s$). Its validity has been demonstrated by Vizet and Ossikovski [19], in reflection at normal incidence, utilizing optical components such as waveplates as well as biological specimens. Furthermore, the assumption $d_1 \approx d_2$ follows from rotational invariance at normal incidence, whereas $M_{R1} \approx M_{R2} = M_R$ results from the (approximate) equivalence of forward/backward propagation (in reflection; M_{R2} being replaced by its transpose) or from the invariance with respect to light reversal (in transmission) still at normal incidence.

Furthermore, $d_1 \approx d_2$ and $M_{R1} \approx M_{R2} = M_R$ [19], where M_R is the Mueller matrix of a linear retarder with retardance δ and azimuth of the optical axis of linear birefringent medium θ , equation (7). Unlike the LC and differential decompositions, in the 3×4 decomposition the retarder M_R is explicitly assumed to be linear ($M_R = M_{RL}$). This assumption is justified for an essentially homogeneous medium (effectively behaving either as an optically thick single layer or a semi-infinite substrate) lacking (or, more generally, having negligible) optical activity. Conversely, the actual 3×4 decomposition cannot be applied to multilayer structures since those generally behave as elliptical retarders:

$$M_R = \begin{bmatrix} 1 & 0^T \\ 0 & m_R \end{bmatrix}, \quad (7a)$$

$$m_R = \begin{bmatrix} m_{11} & m_{12} & m_{13} \\ m_{12} & m_{22} & m_{23} \\ -m_{13} & -m_{23} & m_{33} \end{bmatrix}. \quad (7b)$$

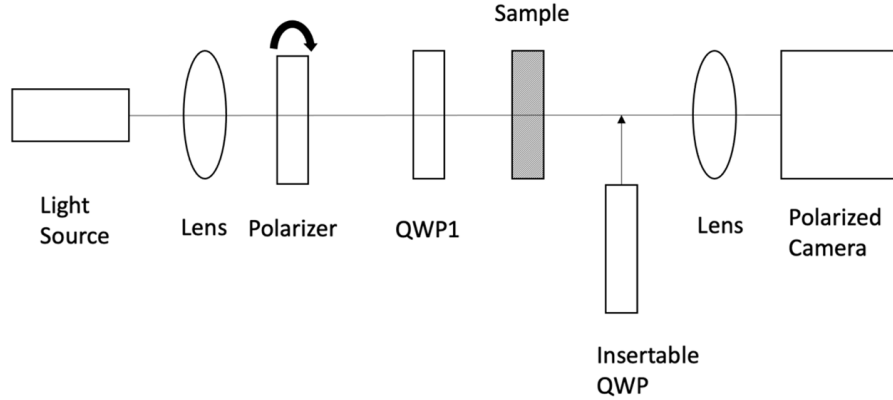


Figure 1. Experimental setup consisting of a light source with collimating lens, a PSG consisting of a polarizer on a rotational stage, a quarter-wave plate (QWP1), and PSA utilizing the polarized camera with lens and a quarter wave plate (QWP) that is inserted only when measuring the 4×4 Mueller Matrix.

Therefore, a diattenuation-free Mueller matrix M can describe the experimental configuration:

$$M \approx M_R M_{\Delta d} M_R, \quad (8)$$

that is dependent on four parameters: two depolarization coefficients, d_1 and d_3 , retardance δ , and azimuth θ .

Taking into account five of the twelve effectively measured Mueller matrix elements from the first three rows, the following set of equations can be written:

$$M_{22} = d_1 m_{11}^2 + d_2 m_{12}^2 - d_3 m_{13}^2 \quad (9a)$$

$$M_{23} = (d_1 m_{11} + d_2 m_{22}) m_{12} - d_3 m_{13} m_{23} \quad (9b)$$

$$M_{24} = d_1 m_{11} m_{13} + d_2 m_{12} m_{23} + d_3 m_{13} m_{33} \quad (9c)$$

$$M_{33} = d_1 m_{12}^2 + d_2 m_{22}^2 - d_3 m_{23}^2 \quad (9d)$$

$$M_{34} = d_1 m_{12} m_{13} + d_2 m_{22} m_{23} + d_3 m_{23} m_{33}, \quad (9e)$$

where m_{ij} ($i, j = 1, 2, 3$) are the elements of matrix m_R from equation (8).

Equation (9) represent an overdetermined set of five equations to solve for four unknown parameters: d_1 , d_3 , δ and θ .

These four parameters are obtained by solving equations (9a)–(9e) with a Nelder–Mead Simplex minimization method implemented in MATLAB (MathWorks, Natick, MA).

2.1. Validation

This approach was validated experimentally with the setup shown in figure 1. The reduced 3×4 Mueller matrix polarimeter consists of a 625 nm LED (M625L3, Thorlabs

Inc., Newton, NJ) source coupled with a linear polarizer (LPVISC100, Thorlabs Inc., Newton, NJ) housed in a rotational stage with a PSG of horizontal, vertical, 45 degrees and the addition of a quarter wave plate (QWP) (AQWP05M-580, Thorlabs Inc., Newton, NJ) to create right circularly polarized light. The PSA consists of a polarized camera (CS505MUP, Thorlabs Inc., Newton, NJ). A QWP (AQWP05M-580, Thorlabs Inc., Newton, NJ) could be inserted into the detection arm in order to analyze circularly polarized light component and create a full 4×4 Mueller matrix. This setup was used to image a number of samples, such as polarizers, QWPs and silicone phantoms at various orientations. Moreover, a $5 \mu\text{m}$ thick section of human skin model mounted on a glass slide with parallel collagen fiber alignment along the dermis [25] was also imaged by adding a 2X objective lens (Mitutoyo Plan Apo, Mitutoyo America Crop, IL) to the PSA.

The system was calibrated as previously reported by Saytashev *et al* [26], yielding an error of less than 3% in the calculation of an identity Mueller matrix of air. The condition number for our system was equal to 4.5.

3. Results and discussion

3.1. Error analysis

The values of the elements of Mueller matrix are dependent on the input variables: d_1 , δ , θ and d_3 (as seen in equation (9e)). Understanding the intrinsic error of the minimization algorithm used for the decomposition of 3×4 reduced Mueller matrix (as it pertains to these variables) is useful to determine the limitations of using such approach. In order to conduct an error analysis, three input variables, d_1 , δ and θ (d_3 was kept constant), were used to calculate a Mueller matrix MMpre (equation (8)) within a range of values for each variable (i.e. δ and θ varied from 0° to 180° and d_1 varied from 0 to 1). The five elements of calculated Mueller matrix were then used for the solution of equation (9) by minimization. The same three variables were obtained and used

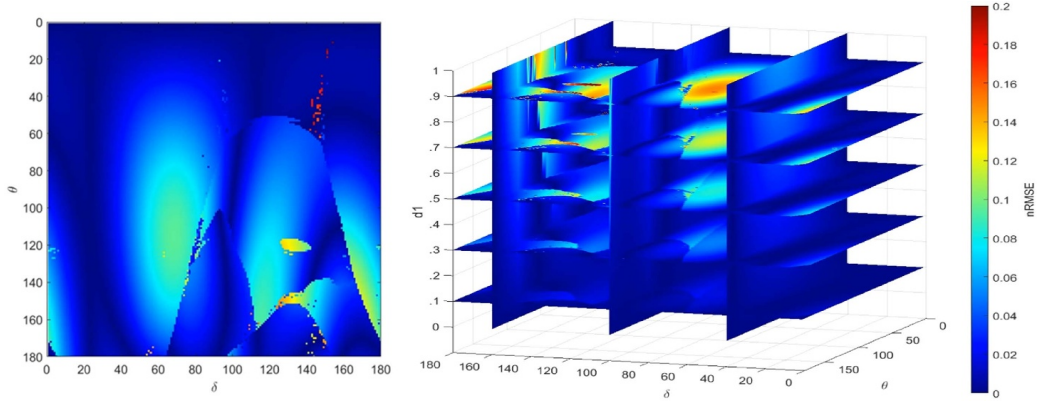


Figure 2. Error analysis of the minimization algorithm used for the decomposition of a reduced 3×4 Mueller matrix. The left figure shows a slice of error values for all θ and δ with d_1 fixed at 0.7. The right figure shows the error contour plots in selected volume sections.

to calculate a new Mueller matrix MM_{post} (equation (8)). The error of the minimization algorithm was estimated by calculating the normalized root mean square error (nRMSE) of the difference between the two Mueller matrices (MM_{pre} and MM_{post}). The nRMSE values vary between 0 and 1, where 0 yields no difference between the values of two Mueller matrices MM_{pre} and MM_{post} . Figure 2 shows a sample slice of the error encountered upon minimization for all θ and δ with d_1 fixed at 0.7 (left panel) and a closer look at selected cross-sections from the overall volume of values (right panel) for better visualization of the error. There is a peak error value of 18% for high values of θ (>100 degrees) and d_1 (>0.7) and arbitrary δ values, although the mean error value for the entire volume was 2.5%.

3.2. Decomposition implementation

We first aimed to compare the different decompositions using an experimentally recorded Mueller matrix M (equation (10d)) introduced by Ghosh *et al* [1] with a known depolarization, retardance, diattenuation and θ values. The polar LC decomposition was applied first to the 4×4 matrix M (which takes into account all three polarization parameters), then the decomposition of the reduced 3×4 matrix was applied using the depolarization and retardance matrix (since our assumption is that M_D is unity), as seen in equation (8). For the comparison, the D decomposition of the complete 4×4 matrix M was also tested.

The values of the depolarization, the retardance and the azimuth of the optical axis calculated using matrix M and the above-mentioned decompositions are listed in table 1:

$$M = \begin{bmatrix} 1 & -0.0229 & 0.0027 & 0.0058 \\ -0.0186 & 0.9956 & -0.0361 & 0.0318 \\ -0.0129 & 0.0392 & 0.2207 & -0.9656 \\ 0.0014 & 0.0280 & 0.9706 & 0.2231 \end{bmatrix} \quad (10a)$$

Table 1. The decomposition parameters (Δ , δ , θ) for the matrix M (equation (10)). (First column) values from Ghosh *et al* [1], (second column) values from the LC decomposition, (third column) D decomposition and (fourth column) decomposition of the reduced 3×4 matrix.

	Ghosh <i>et al</i>	4×4 LC	4×4 D	3×4
Parameters	Estimated values			
Δ	0.005	0.005	0.005	0.005
δ (rad)	1.346	1.345	1.346	1.346
θ (deg)	89.05	89.94	0.013	89.98

$$M_{\Delta} = \begin{bmatrix} 1 & 0 & 0 & 0 \\ 0.0041 & 0.9969 & 0 & 0 \\ -0.0070 & 0 & 0.9915 & 0 \\ -0.0019 & 0 & 0 & 0.9966 \end{bmatrix} \quad (10b)$$

$$M_R = \begin{bmatrix} 1 & 0 & 0 & 0 \\ 0 & 0.9988 & -0.0362 & 0.0281 \\ 0 & 0.0393 & 0.2207 & -0.9741 \\ 0 & 0.0320 & 0.9742 & 0.2239 \end{bmatrix} \quad (10c)$$

$$M_D = \begin{bmatrix} 1 & -0.0229 & 0.0027 & 0.0058 \\ -0.0229 & 1.000 & -0.000 & -0.0001 \\ 0.0027 & 0.000 & 0.9997 & 0.000 \\ 0.0058 & -0.0001 & 0.0000 & 0.9997 \end{bmatrix}. \quad (10d)$$

The results of the different decompositions of a complete 4×4 matrix M and its reduced 3×4 version yielded a similar answer to what has been previously reported [1, 27]. The decomposition of a reduced 3×4 Mueller matrix matches its 4×4 counterparts for this low-depolarizing medium, noting the only difference in the 4×4 D is the orientation being equal to $(|\theta - 90|)$.

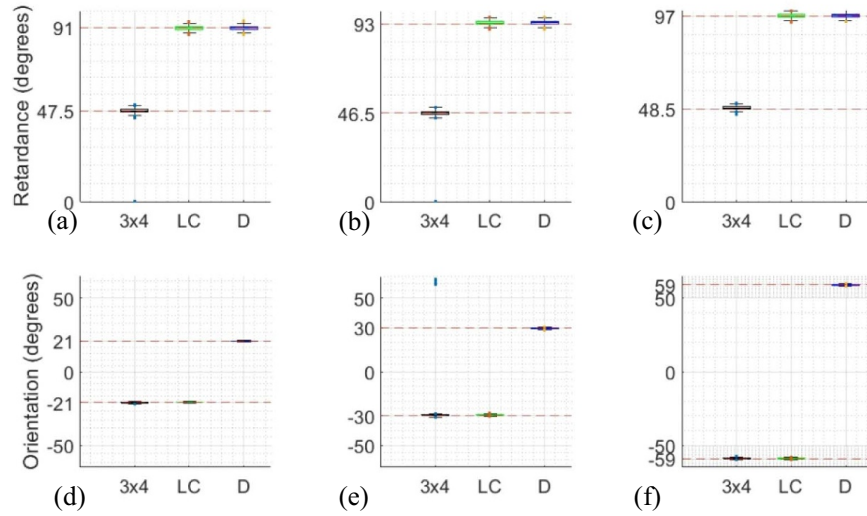


Figure 3. Comparison between the decomposition of a reduced 3×4 Mueller matrix (3×4), LC and D decompositions of 4×4 Mueller matrix of the QWPs oriented at (a, d) -20 degrees, (b, e) -30 degrees and (c, f) -60 degrees with respect to the polarization axis of the incident beam. The red lines delineate the median value of the data set.

To further investigate the proposed decomposition of a reduced 3×4 Mueller matrix, a QWP with its axis oriented at three different angles: -20 , -30 and -60 degrees—assuming the frame of reference to be the benchtop plane—was imaged. The QWP is a retarding element with theoretically neither depolarization nor diattenuation present, therefore we can focus on the new decomposition method’s response to retardance and azimuth of orientation.

The parameters calculated with all decompositions of the Mueller matrix of the QWP measured at different azimuth angles can be observed in figure 3, where the complete 4×4 experimentally recorded Mueller matrix was used to calculate the LC and D decompositions and the first three rows of this Mueller matrix were used to calculate the 3×4 decomposition. There is a wide agreement within the three decomposition methods on the orientation angle values for all measurements, showing the QWP positioned at -20 degrees (#a, d), -30 degrees (#b, e) and -60 degrees (#c, f). The retardance of QWP calculated with the reduced 3×4 Mueller matrix decomposition appears as half of the value compared to the values calculated with its 4×4 counterparts at different QWP orientations. This discrepancy is likely due to the absence of depolarization, modifying our definition of the 3×4 matrix decomposition (equation (8)) to equal $M \approx M_R^2$. Moreover, the lack of the fourth row in the reduced 3×4 Mueller matrix leads to a negative retardance value in some cases, which causes the angle to be shifted by 90 degrees. A correction for this is necessary, entailing of modifying the orientation angle by 90° each time a negative retardance is obtained (correction for this was already applied in figure 3). The QWP orientation angle agreed well for all positions, matching the 3×4 decomposition with the 4×4 LC decomposition in every measurement, as well as the orientation angle value calculated with the D decomposition but with a differing sign.

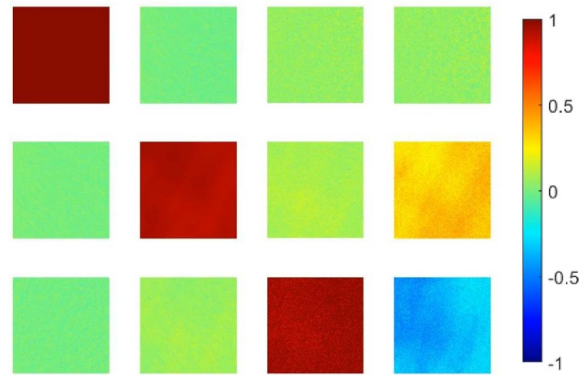


Figure 4. Reduced 3×4 Mueller matrix of a silicone sample oriented at -70 degrees, showing the striation direction. The weakly depolarizing nature of the sample is confirmed by the dominance of the diagonal values that are close to one.

Looking further into comparing the decompositions experimentally, an extruded silicone phantom consisting of a silicone strip with visible striations along the direction of extrusion, oriented at three different positions was imaged with our setup. A low depolarization and uniform retardance is expected due to its natural semitransparent characteristics. The reduced 3×4 Mueller matrix of the silicone phantom oriented at -70 degrees can be observed in figure 4, demonstrating the structured striations and weakly depolarizing nature of the sample.

The results of the decomposition of the Mueller matrix of the aforementioned phantom with different algorithms can be seen in figure 5, where we can qualitatively see the similar values of depolarization, the values of the retardance calculated

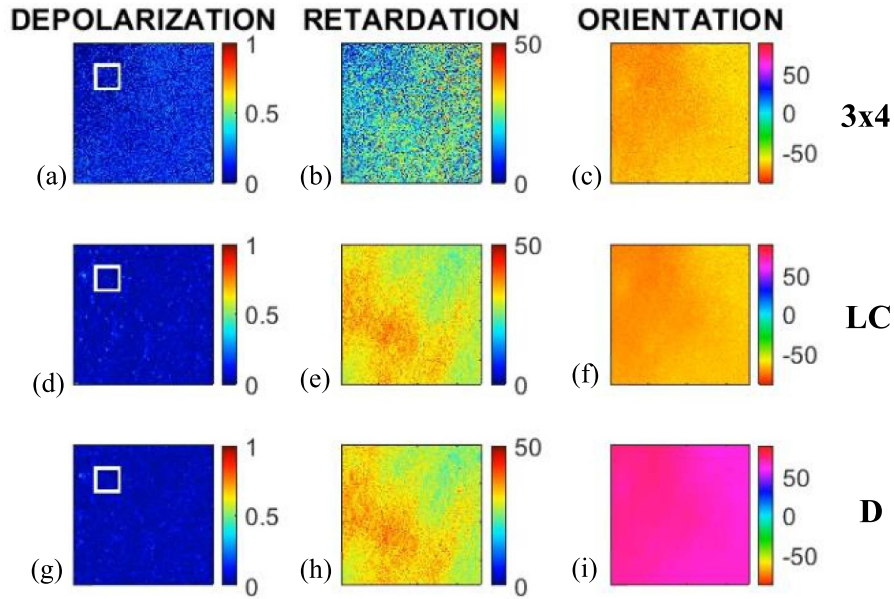


Figure 5. The images of (a, d, g) the depolarization, (b, e, h) the retardance and (c, f, i) the angle of orientation calculated from Mueller matrix of a silicone phantom oriented at -70 degrees using the three decomposition methods: (first row) 3×4 decomposition, (second row) LC decomposition, and (third row) D decomposition. The white box indicates a region of interest at which the sample is assumed to be homogeneous (for comparison purposes).

with 3×4 decomposition close to half of the retardance values calculated with the decompositions of the complete 4×4 Mueller matrix and the agreement on the orientation angle for all decompositions. The white box in the figure 5 indicates a 30×30 pixel region of interest (ROI) where the sample is assumed to be homogeneous to fairly compare the three decomposition methods.

To more quantitatively ascertain the decomposition methods, the calculated depolarization, retardance and orientation angle values for the silicone phantom (within the selected ROI) oriented at -70 , -60 and 80 degrees are shown in figure 6.

At all measurement configurations the silicone phantom shows a similar distribution of depolarization values within the selected ROI, ranging from 0 to 0.35, with a median value around 0.2 calculated with the 3×4 decomposition (figures 6(a)–(c)), although notably different from the distributions of depolarization values calculated with both LC and D decompositions of the complete 4×4 Mueller matrix (median value is 0.04). This could be due to the difference in the depolarization definitions for the different calculations. The distribution of the retardance values calculated with the reduced 3×4 Mueller matrix decomposition (figure 6(d)) offers a wider set of data points than the 4×4 methods (figures 6(e) and (f)), with the median value falling close to the half-retardance mark of the calculated retardance value for the latter. This phenomenon is due to the low depolarization of the silicon phantom, similarly to that of the quarter-wave plate in the previous experiment. As for the

orientation angle (figures 6(g)–(i)), we notice a similitude between the distributions of the angle values (and range of angles perceived) for the reduced 3×4 Mueller matrix decomposition and the LC decomposition. The D decomposition shows an opposite sign of angle in all cases. This difference in sign for the D decomposition is due its definition and the use of different matrix elements (compared to the LC) used to calculate the orientation.

Lastly, the results of different decompositions of the Mueller matrix of the section of human skin model mounted on the glass slide can be seen in figure 7 and summarized in the boxplots in figure 8. This sample is also weakly depolarizing (due to its small thickness of $5 \mu\text{m}$) and shows a similar pattern as the previous samples for the retardance values, where the reduced 3×4 Mueller matrix decomposition values are found to be about half of the values calculated with LC and D decompositions of the complete 4×4 Mueller matrix. The orientation angle of the sample is in agreement for the 3×4 and the LC decompositions, although it appears to be the complement angle ($|\theta - 90|$) for the D decomposition.

Similar distributions of the depolarization values within the selected ROI are calculated with all three decompositions. The values of retardance calculated with the reduced 3×4 Mueller matrix decomposition are found to be about half of the values calculated with LC and D decompositions of the complete 4×4 Mueller matrix as for the silicon phantom. The same trends are observed for the distributions of the orientation angle calculated with three different decompositions as in case of the silicon phantom.

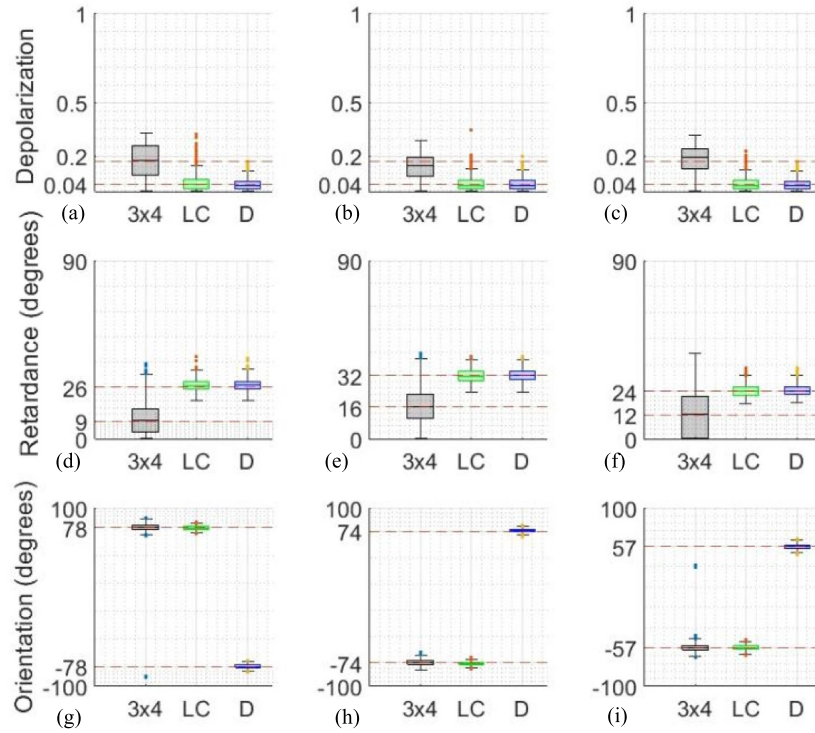


Figure 6. Comparison between the reduced 3×4 Mueller matrix decomposition, LC and D decompositions of the complete 4×4 Muller matrix of silicone phantom oriented at (a, d, g) 80 degrees, (b, e, h) 70 degrees and (c, f, i) 60 degrees with respect to the reference plan of the incident beam. The red lines delineate the median values within the ROI.

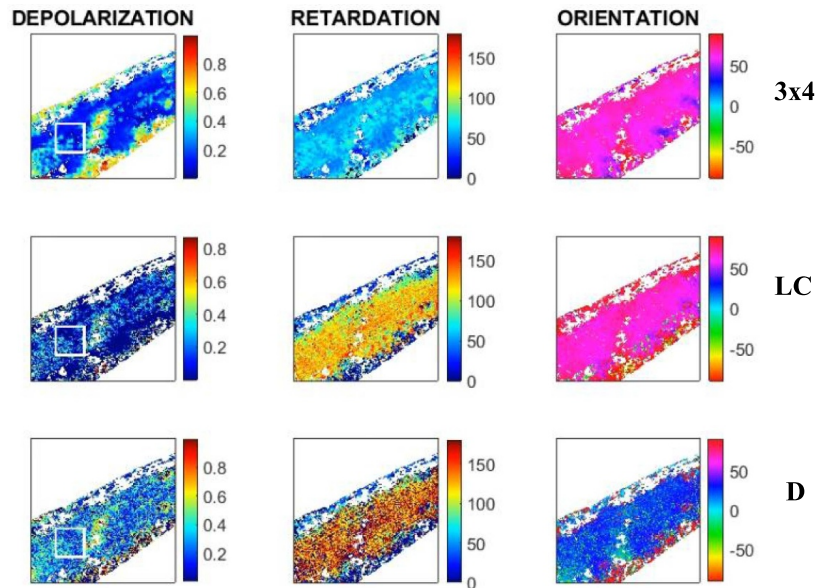


Figure 7. The images of the depolarization, the retardance and the orientation angle of human skin model section mounted on the glass slide with focus on the dermis. The parameters calculated with three different decompositions: 3×4 , LC and D are shown from top to bottom, respectively. The saturated and background pixels have been rendered in white. The white box indicates a region of interest in the dermis at which the sample is assumed to be homogeneous.

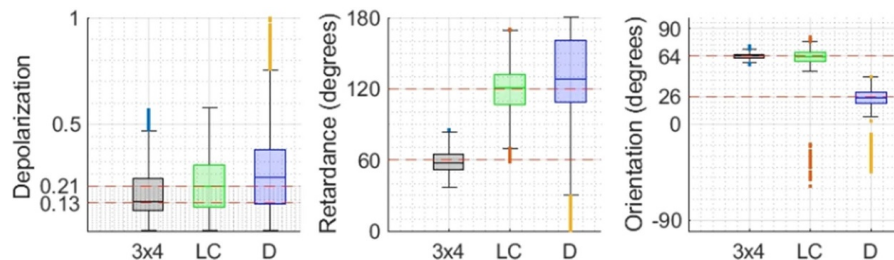


Figure 8. Comparison of the results of three decompositions of the Mueller matrix of human skin model section, where we can observe the similitude of the 3×4 decomposition with the 4×4 LC decomposition as well as the D. Red lines indicate median value of the data set.

4. Conclusion

This paper introduces a new method of decomposition for a reduced 3×4 Mueller matrix. This decomposition has shown to be capable of calculating the correct polarimetric parameters (depolarization, retardance and orientation angle) when compared to the established decomposition methods of the complete 4×4 Mueller matrix. The decomposition of the previously reported Mueller matrix (equation (10)) for the 4×4 decompositions and the diattenuation free matrix (only using equation (10c)) yielded similar values to what were reported by the authors for all polarimetric parameters. For the experimental cases shown, the depolarization values did not yield similar values, likely due to the difference in depolarization factor definition for all three decompositions methods. The retardance values calculated with the new decomposition were approximately equal to half the retardance values calculated with the LC and D decompositions of the complete 4×4 Mueller matrix for all the cases, which is due to the definition of the 3×4 decomposition (equation (8)). The orientation angle, values calculated with the new decomposition were aligned well with the values calculated with the decompositions of the complete 4×4 Muller matrix (especially with the LC decomposition) in all samples. Discrepancies in the orientation angle values shown for the D decomposition are due to the matrix elements used to calculate the orientation angle value. Taking into account inherent errors due to the minimization algorithm used, further testing with a wider array of samples with differing polarization properties needs to be conducted to understand what limitations these errors could pose. Moreover, we plan to explore the behavior of the new decomposition of the reduced 3×4 Mueller matrix for more depolarizing samples, since this is a property exhibited by biological tissues.

This new decomposition method of the reduces 3×4 Mueller matrix has a particular value due to the technological advances giving rise to polarization cameras, as it will help to omit the need for circular polarization analysis components in the PSA and therefore to simplify the experimental setup needed for the full characterization of sample using Mueller matrix polarimetry. This simplification could provide a fast and robust solution to current uses of polarimetry, especially in a clinical setting where time and simplicity poses an issue.

Data availability statement

The data generated and/or analysed during the current study are not publicly available for legal/ethical reasons but are available from the corresponding author on reasonable request.

Acknowledgments

The authors are grateful to Dr Christian Lotz, Dr Florian Kai Groeber-Becker and Dr Sofia Dembski from the Fraunhofer Institute for Silicate Research ISC, Translational Center for Regenerative Therapies, Würzburg, Germany for providing the samples of human skin model. Dr Ramella-Roman acknowledges the funding of National Science Foundation (DMR 1548924).

ORCID iDs

Mariacarla Gonzalez  <https://orcid.org/0000-0002-0541-4857>

Razvigor Ossikovski  <https://orcid.org/0000-0002-7084-7579>

Tatiana Novikova  <https://orcid.org/0000-0002-9048-9158>

Jessica C Ramella-Roman  <https://orcid.org/0000-0002-5710-6004>

References

- [1] Ghosh N, Wood M F G and Vitkin I A 2008 Mueller matrix decomposition for extraction of individual polarization parameters from complex turbid media exhibiting multiple scattering, optical activity, and linear birefringence *J. Biomed. Opt.* **13** 1–14
- [2] Goldstein D H 2011 *Polarized Light* p 808
- [3] Ghosh N and Vitkin A I 2011 Tissue polarimetry: concepts, challenges, applications, and outlook *J. Biomed. Opt.* **16** 30
- [4] Novikova T 2017 Optical techniques for cervical neoplasia detection *Beilstein J. Nanotechnol.* **8** 1844–62
- [5] Ramella-Roman J C, Saytashev I and Piccini M 2020 A review of polarization-based imaging technologies for clinical and preclinical applications *J. Opt.* **22** 123001

- [6] Atkinson G A and Ernst J D 2018 High-sensitivity analysis of polarization by surface reflection *Mach. Vis. Appl.* **29** 1171–89
- [7] Qi J, He C and Elson D S 2017 Real time complete Stokes polarimetric imager based on a linear polarizer array camera for tissue polarimetric imaging *Biomed. Opt. Express* **8** 4933–46
- [8] Ma X et al 2018 Pixelated-polarization-camera-based polarimetry system for wide real-time optical rotation measurement *Sens. Actuators B* **283** 857–64
- [9] David R, Maik R and Gunther N 2019 Principle investigations on polarization image sensors *Photon. Educ. Meas. Sci.* **11** 144
- [10] Nathan H, Shuhei S and Yukitoshi O 2019 Generating high-performance polarization measurements with low-performance polarizers: demonstration with a microgrid polarization camera *Opt. Eng.* **58** 1–4
- [11] Nathan A H, Shuhei S and Yukitoshi O 2019 Calibration and performance assessment of microgrid polarization cameras *Opt. Eng.* **58** 1–9
- [12] Ren H, Yang J, Liu X, Huang P and Guo L 2020 Sensor modeling and calibration method based on extinction ratio error for camera-based polarization navigation sensor *Sensors* **20** 3779
- [13] Sarkar M, Segundo Bello D S, Van Hoof C and Theuwissen A 2010 Biologically inspired autonomous agent navigation using an integrated polarization analyzing CMOS image sensor *Proc. Eng.* **5** 673–6
- [14] Wood T C and Elson D S 2010 Polarization response measurement and simulation of rigid endoscopes *Biomed. Opt. Express* **1** 463–70
- [15] Lu S-Y and Chipman R A 1996 Interpretation of Mueller matrices based on polar decomposition *J. Opt. Soc. Am. A* **13** 1106–13
- [16] Satish K et al 2012 Comparative study of differential matrix and extended polar decomposition formalisms for polarimetric characterization of complex tissue-like turbid media *J. Biomed. Opt.* **17** 1–12
- [17] Ossikovski R, De Martino A and Guyot S 2007 Forward and reverse product decompositions of depolarizing Mueller matrices *Opt. Lett.* **32** 689–91
- [18] Ossikovski R 2009 Analysis of depolarizing Mueller matrices through a symmetric decomposition *J. Opt. Soc. Am. A* **26** 1109–18
- [19] Vizet J and Ossikovski R 2018 Symmetric decomposition of experimental depolarizing Mueller matrices in the degenerate case *Appl. Opt.* **57** 1159–67
- [20] Ortega-Quijano N and Arce-Diego J L 2011 Mueller matrix differential decomposition *Opt. Lett.* **36** 1942–4
- [21] Ossikovski R 2011 Differential matrix formalism for depolarizing anisotropic media *Opt. Lett.* **36** 2330–2
- [22] Swami M K, Manhas S, Buddhiwant P, Ghosh N, Uppal A and Gupta P K 2006 Polar decomposition of 3×3 Mueller matrix: a tool for quantitative tissue polarimetry *Opt. Express* **14** 9324–37
- [23] Qi J, Ye M, Singh M, Clancy N T and Elson D S 2013 Narrow band 3×3 Mueller polarimetric endoscopy *Biomed. Opt. Express* **4** 2433–49
- [24] Wang Y et al 2015 Study on the validity of 3×3 Mueller matrix decomposition *J. Biomed. Opt.* **20** 1–7
- [25] Lee H R et al 2018 Mueller microscopy of anisotropic scattering media: theory and experiments *Proc. SPIE* **10677** 1067718
- [26] Saytashev I, Saha S, Chue-Sang J, Lopez P, Laughrey M and Ramella-Roman J C 2020 Self validating Mueller matrix micro-mesoscope (SAMMM) for the characterization of biological media *Opt. Lett.* **45** 2168–71
- [27] Ghosh N Correction on reported depolarization values for Ghosh et al JBO 2008 Table 1 reported depolarization $\delta = 0.995$ should be $\delta = 0.005$ 2021